scientific reports

Check for updates

OPEN

# Role of T cell exhaustion and tissue-resident memory T cells in the expression and prognosis of colorectal cancer

Han Wu[1,2], Pei-Wen Fan[1,2], Ya-Ning Feng[1,2], Cheng Chang[3,4], Ting Gui[1,2], Jia-bei Meng[1,2] & Ruo-Zheng Wang[1,2,3,4]✉

**The tumour microenvironment (TME) is complex and dynamic, and changes significantly with tumour progression. Studying the evolving state of T cells, especially tumour-specific subsets, has become feasible. However, the roles of exhausted T cells (Tex) and pre-exhausted tissue-resident memory T cells (pf-Trm), which emerge after prolonged antigen stimulation, remain unclear. Using single-cell sequencing data, we analyzed the immune landscape of patients with colorectal cancer (CRC) across clinical stages to quantify the abundance of T cell subtypes. Functional enrichment analysis revealed that early stage Tex cells retained some functionality, whereas advanced stage Tex cells showed a significant functional loss. Early stage pf-Trm cells actively participate in immune surveillance and antigen presentation, whereas advanced stage pf-Trm cells exhibit reduced functions. Flow cytometry analysis of clinical cohorts was used to measure the proportions of Tex and pf-Trm. Elevated levels of PD-1 and Tim-3 have been detected in TILs from CRC patients. Data from The Cancer Genome Atlas (TCGA) linked high Tex levels to poor prognosis in CRC, while pf-Trm correlated with better outcomes in early CRC but worse outcomes in advanced CRC due to functional exhaustion. Thus, Tex and pf-Trm cells may serve as prognostic biomarkers, and Tim-3 and CD103 may be promising targets for immune checkpoint inhibitors.**

**Keywords** Colorectal cancer, Tumour microenvironment, T-cell exhaustion, Pre-failure tissue-resident memory T cells, Clinical prognosis

**Abbreviations**

| | |
|---|---|
| BP | Biological Process |
| CD39 (protein) | Ectonucleoside triphosphate diphosphohydrolase 1 (ENTPD1,gene) |
| CD103 (protein) | Integrin subunit alpha E (ITGAE, gene) |
| CRC | Colorectal cancer |
| ENTPD1 (gene) | Ectonucleoside triphosphate diphosphohydrolase 1 (CD39,protein) |
| GO | Gene Ontology |
| HAVCR2 (gene) | Hepatitis A virus cellular receptor 2 (Tim-3,protein) |
| ITGAE (gene) | Integrin subunit alpha E (CD103,protein) |
| ICIs | Immune checkpoint inhibitors |
| KEGG | Kyoto Encyclopedia of Genes and Genomes |
| MIF | Macrophage migration inhibitory factor |
| MLH1Meth | MLH1 promoter methylated |
| MLH1NoMeth | MLH1 promoter unmethylated |
| MSI | Microsatellite instability |

[1]Xinjiang Key Laboratory of Oncology, The Third Affiliated Teaching Hospital (Affiliated Cancer Hospital) of Xinjiang Medical University, Urumqi 830011, Xinjiang, China. [2]State Key Laboratory of Pathogenesis, Prevention and Treatment of High Incidence Diseases in Central Asia, Departments of Institute for Cancer Research, The Third Affiliated Teaching Hospital (Affiliated Cancer Hospital) of Xinjiang Medical University, Urumqi 830011, Xinjiang, China. [3]Clinical Key Specialty of Radiotherapy, Health and Welfare Commission, Urumqi 830011, Xinjiang, China. [4]Xinjiang Clinical Research and Cultivation Center for Cancer Radiotherapy, Urumqi 830011, Xinjiang, China. ✉email: wrz8526@vip.163.com

| | |
|---|---|
| MSS | Microsatellite stable |
| NK | Natural killer cells |
| OS | Overall survival |
| P | Peritumoural tissue |
| PBMC | Peripheral blood mononuclear cells |
| PD-1 (protein) | Programmed cell death protein 1 (PDCD1,gene) |
| PDCD1 (gene) | Programmed cell death protein 1 (PD-1,protein) |
| pf-Trm | Precursor exhausted tissue-resident memory T cells |
| RFS | Relapse-free survival |
| scRNA-seq | Single-cell RNA sequencing |
| T | Tumour tissue |
| TCGA | The Cancer Genome Atlas |
| Tex | Terminally exhausted T cells |
| TIL | Tumour-infiltrating lymphocyte |
| Tim-3 (protein) | Hepatitis A virus cellular receptor 2 (HAVCR2,gene) |
| TME | Tumour microenvironment |
| TPM | Transcripts per million |
| Trm | T |
| issue-resident memory T cells | |
| t-SNE | t-distributed stochastic neighbor embedding |
| UALCAN | University of Alabama at Birmingham Cancer Data Analysis Portal |
| UMAP | Uniform Manifold Approximation and Projection |
| Z-score | Standard score |

Colorectal cancer (CRC) is the most common malignancy of the gastrointestinal tract and remains a leading cause of cancer-related mortality worldwide. It currently ranks as the second most frequent cause of cancer-related deaths, posing a major global public health challenge[1,2]. The tumour microenvironment (TME) plays a central role in cancer progression. Tumour cells engage in dynamic interactions with their surroundings by releasing signalling molecules, promoting angiogenesis, and inducing immune tolerance, thereby facilitating metastasis. Components of the TME—including lymphocytes, fibroblasts, myeloid-derived suppressor cells (MDSCs), the extracellular matrix, and non-cellular factors—modulate tumour growth and dissemination to secondary organs[3–5].The abundance and functional status of T cells within the TME vary across cancer types, shaped by distinct immunoregulatory mechanisms[6,7]. Tumour heterogeneity and the complex immunosuppressive milieu promote immune evasion and tumour progression via multiple inhibitory pathways[8].

Although T cell exhaustion is often associated with impaired immune responses, it arises in the context of prior activation and may serve as a mechanism to regulate chronic inflammation and prevent tissue damage[9]. Programmed death-1 (PD-1), a hallmark of T cell exhaustion, is also expressed on multiple T cell subsets, including tissue-resident memory T cells (Trm), and thus does not invariably indicate a dysfunctional or prognostically unfavourable phenotype[10,11]. Trm cells are crucial for local immune surveillance and have demonstrated potent anti-tumour activity, including enhanced cytotoxicity and proliferative capacity in lung cancer patients responding to immunotherapy[12]. High Trm infiltration has been linked to improved survival and better responses to immunotherapy in cancers such as melanoma, ovarian cancer, and intrahepatic cholangiocarcinoma[13–16]. Notably, Trm cells are heterogeneous and express multiple immune checkpoints such as PD-1 and Tim-3, making them attractive targets for immune checkpoint blockade therapies[17,18].

$CD8^+$ T cells co-expressing PD-1 and CD103, with or without Tim-3, comprise heterogeneous subsets with distinct differentiation states and effector capacities, broadly categorised as exhausted T cells or precursor exhausted Trm cells[19,20]. Furthermore, Duhen et al. identified ENTPD1—which encodes the ectonucleotidase CD39—as one of the most differentially expressed genes between $CD103^+$ and $CD103^-$ $CD8^+$ tumour-infiltrating lymphocytes (TILs)[21]. Growing evidence indicates that $CD39^+CD8^+$ T cells are enriched for tumour reactivity, and that CD39 serves as a robust marker of T cell activation within the TME[22,23]. Importantly, CD39 expression can distinguish tumour-reactive $CD8^+$ T cells from bystander $CD8^+$ T cells, positioning it as a key surface marker for identifying tumour-specific T cells[24,25].

Identifying exhaustion-associated markers and understanding their functional significance in the heterogeneity of the tumor–immune microenvironment are critical for advancing cancer immunotherapy. Given the established dichotomy whereby $CD39^-$ $CD8^+$ T cells act as inert bystanders and $CD39^+$ $CD8^+$ T cells exhibit tumor reactivity, we further stratified $CD8^+$ T cells based on exhaustion and residency phenotypes. Specifically, we defined $PD\text{-}1^+$ $Tim\text{-}3^-$ $CD103^+$ $CD8^+$ T cells as precursor exhausted tissue-resident memory T cells (pf-Trm) and $PD\text{-}1^+$ $Tim\text{-}3^+$ $CD103^+$ $CD8^+$ T cells as terminally exhausted T cells (Tex) to investigate their respective roles in colorectal cancer (CRC) progression. In the early phase of our study, we conducted a systematic literature review and a series of experiments to characterize multiple exhaustion- and activation-related checkpoints—including LAG-3, TIGIT, CTLA-4, ICOS, and 4-1BB—in tumor-infiltrating $CD8^+$ T cells. Although these additional markers were expressed and modulated T cell functional states to some extent, their ability to discriminate between exhaustion states—and their demonstrated biological relevance in our preliminary data—was moderately inferior to that of the PD-1/Tim-3 combination. Therefore, to ensure model robustness and focus on the most discriminatory and prognostically validated markers in CRC, we retained PD-1, Tim-3, CD39, and CD103 as our core analytical markers.

In this study, we conducted a comprehensive phenotypic and functional analysis of peripheral and intratumoural T cells from CRC patients using flow cytometry and public single-cell transcriptomic datasets. We also performed computational analyses on both single-cell and bulk transcriptomic data from published CRC

cohorts. Our aim was to delineate the phenotypic architecture and functional heterogeneity of tumour-reactive ($CD39^+$), bystander ($CD39^-$), and distinct subsets of exhausted $CD8^+$ T cells—including terminally exhausted T cells (Tex) and pre-failure tissue-resident memory T cells (pf-Trm)—throughout the progression of CRC. By leveraging single-cell transcriptomics and clinical stratification, we aim to define how these immunological states evolve in the TME across disease stages, and to elucidate their associations with tumour dynamics and patient prognosis. This work provides mechanistic insight into the shifting immune landscape in CRC and establishes a conceptual framework for stage-specific immune surveillance and therapeutic targeting.

## Materials and methods

### Patient cohort and samples

Between November 2021 and December 2023, a consecutive cohort of 40 treatment-naïve CRC patients was prospectively enrolled at the Affiliated Cancer Hospital of Xinjiang Medical University. Eligible participants met all of the following inclusion criteria: (1) histologically confirmed primary CRC; (2) no prior antitumour therapy; (3) Karnofsky Performance Status (KPS) ≥ 80; and (4) planned curative surgery with informed consent. Exclusion criteria included secondary malignancies, hereditary CRC syndromes (e.g., Lynch syndrome or familial adenomatous polyposis), or incomplete clinical data.

Due to excessive signal noise, insufficient cell event counts, and challenges in obtaining peripheral blood samples, we ultimately collected 37 tumor tissue specimens, 40 adjacent normal tissue specimens (defined as histologically confirmed normal mucosa located ≥ 5 cm from the tumor margin), and 22 pre-treatment peripheral blood samples, all prior to any therapeutic intervention.Written informed consent was obtained from all participants in accordance with ethical guidelines.Comprehensive clinicopathological data were gathered for all patients, including demographic characteristics (age, sex), tumour location, and detailed TNM staging (Table 1). This study was conducted in accordance with the Declaration of Helsinki and was approved by the Medical Ethics Committee of the Cancer Hospital Affiliated to Xinjiang Medical University (Approval No. K-2021005). The 8th edition of the AJCC on Cancer tumour-node-metastasis (TNM) system.

This study included two endpoints: overall survival (OS) and disease-free survival (DFS), defined respectively as the interval from surgery to death and from surgery to first documented recurrence. All patients were followed until June 2025, with no deaths or recurrences observed; therefore, neither median OS nor median DFS was reached.

### Cell isolation

Peripheral blood mononuclear cell(PBMCs) were extracted from EDTA-anticoagulated blood samples via Ficoll density gradient centrifugation, and tumour-infiltrating lymphocytes (TILs) were isolated from tumour tissue specimens by mechanical dissociation using a sterile 70 μm cell filter (BD Biosciences, Franklin Lakes, NJ), followed by enzymatic digestion with Enzyme H and Enzyme R to separate lymphocytes from CRC tissues. Lymphocytes isolated from adjacent normal tissue (P) and tumour tissue (T) were counted and their viability was assessed using the trypan blue exclusion method.

| Characteristics | CRC patients($n = 40$) | |
|---|---|---|
| | Numbers | Proportion(%) |
| Gender | | |
| Male | 23 | 57.5% |
| Female | 17 | 42.5% |
| Age (years) | | |
| < 60 | 16 | 40% |
| >= 60 | 24 | 60% |
| Location | | |
| colon | 19 | 47.5% |
| Rectum | 21 | 52.5% |
| Tumour size ($cm^3$) | | |
| < 50 | 32 | 80% |
| >= 50 | 8 | 20% |
| TNM stage | | |
| I ~ II | 21 | 52.5% |
| III ~ IV | 19 | 47.5% |
| Occult Blood | | |
| Yes | 24 | 60% |
| No | 16 | 40% |

**Table 1**. Demographics and clinicopathologic characteristics of the patients with CRC.

### Flow cytometry

Flow cytometry was performed using the following antibodies: anti-human CD3-BUV395, anti-human CD4-PE, anti-human CD8-PerCP-Cy5.5, anti-human PD-1-BV650, anti-human Tim-3-BB515, anti-human CD39-PE-Texas Red, and anti-human CD103-BV711(Supplementary Table 1). Isolated PBMCs and TILs were counted, and $4 \times 10^6$ cells were washed with PBS and resuspended in 1.2 mL of PBS. A 200 µL aliquot was reserved as an unstained control. The remaining cells were stained with 1 µL of Live/Dead™ BV510 dye, incubated at 4 °C for 25 min, washed twice with 2 mL of chilled FACS buffer™, and centrifuged at 1,500 rpm for 5 min at 4 °C. Cells were then resuspended in 80 µL of FACS buffer™, stained with the antibody panel, incubated at 4 °C for 20 min, washed twice with 5 mL of chilled buffer, centrifuged again, and fixed in 200 µL of FACS fix buffer.Data acquisition was performed using a BD FACSFortessa™ cytometer, and analyses were conducted with FlowJo™ software (version 10.8.1).

### Data collection

Single-cell transcriptomic data were obtained from two principal sources: (1) the Gene Expression Omnibus (GEO) database (https://www.ncbi.nlm.nih.gov/geo/), specifically the GSE132465 dataset, comprising 23 CRC cases[20]; and (2) the Single Cell Portal (https://singlecell.broadinstitute.org), specifically the GSE178341 dataset, which includes paired colorectal tumour and adjacent normal tissue samples from 62 patients (28 mismatch repair-proficient [MMR-p] and 34 mismatch repair-deficient [MMR-d] cases)[26]. In addition, bulk transcriptomic data were retrieved from The Cancer Genome Atlas (TCGA) databases (TCGA-COAD and TCGA-READ; https://portal.gdc.cancer.gov/) (Supplementary Table 2).

### Integrated analysis of tumor microenvironment cell types and dynamics in CRC

Single-cell RNA sequencing (scRNA-seq) data of cell types and subtypes within the TME were analysed using the Seurat package. A Seurat object was generated from the gene expression matrix, followed by data normalisation, principal component analysis (PCA), and dimensionality reduction using UMAP. Cell types and subtypes were identified based on canonical marker genes and visualised accordingly. Clustering and differential gene expression analyses were performed using the Wilcoxon rank-sum test, with refinement of specific subtypes achieved through doublet exclusion and dual-round clustering. Pseudotime analysis was conducted using Monocle2 to map cells along developmental trajectories and identify genes exhibiting significant dynamic changes. Cell–cell communication networks were inferred using CellChat software. Differential gene expression analysis was conducted using the FindAllMarkers function within Seurat. Functional enrichment analysis of differentially expressed genes (DEGs) was carried out using the clusterProfiler package, focusing on Gene Ontology (GO) categories and Kyoto Encyclopaedia of Genes and Genomes (KEGG) pathways[27–29].

### Statistical analysis

Statistical analyses were performed using GraphPad Prism v8 (GraphPad Software, USA) and RStudio (RStudio, USA). The Wilcoxon rank-sum test was employed for comparisons between two groups, while the Kruskal–Wallis (K-W) test was used for comparisons across multiple groups. Survival analysis was conducted by systematically evaluating all potential cutoff values within the interquartile range (IQR) of gene expression levels (25th to 75th percentiles). The optimal threshold for distinguishing high- versus low-expression groups was determined by maximising discriminatory power using Kaplan–Meier curve analysis with log-rank testing. Bar graphs display the mean ± standard deviation (SD), and the statistical tests applied are specified in the corresponding figure legends. Statistical significance was indicated as follows: $^*p < 0.05$; $^{**}p < 0.01$; $^{***}p < 0.001$. Data visualisation was performed using FCS Express 7 Research.

## Results

### Annotation and dynamic changes of immune cell subtypes in the CRC TME

To investigate the cellular architecture of the TME in CRC, we analysed publicly available single-cell RNA sequencing (scRNA-seq) data[20]. Details of the pre-processing workflow and cell counts for each cluster are provided in Supplementary Table 3. Following quality control, a total of 47,285 immune cells were retained for unsupervised clustering at a resolution of 0.5 (Supplementary Fig. 1 A). Uniform Manifold Approximation and Projection (UMAP) was subsequently applied to visualise these immune cell populations (Fig. 1A). Marker genes for global cell type annotation included T cells (CD3D, CD3E), NK cells (NCR1), B/pDC cells (CD19, LILRA4), plasma cells (JCHAIN, MZB1), myeloid cells (CD14, FCGR3A, S100A8, S100A9, CSF3R), pericyte/fibroblast/SMC cells (RGS5, PDGFRB, COL3A1, COL1A1, ACTA2, MYH11), endothelial cells (PECAM1), and epithelial cells (EPCAM). The expression patterns of these markers were visualised using bubble plots, and their spatial distribution across clusters was illustrated using UMAP projections (Fig. 1B, Supplementary Fig. 1B). To explore the spatial–temporal dynamics of immune cell populations, we conducted longitudinal profiling across colorectal cancer (CRC) stages. T/NK cells peaked in Stage I (48.3 ± 7.5%), suggesting an active early immune response, but their abundance fell to 34.4 ± 16.7% by Stage III and remained low thereafter. Conversely, epithelial cells—previously characterised as malignant by transcriptomic and proteomic analyses[30,31]—rose steadily to reach 47.7 ± 33.5% in Stage IV, the highest among all stages, while endothelial cells declined to just 0.6 ± 0.9% in Stage IV, the lowest observed. Although these trends align with an immunologically "cold" late-stage microenvironment, nonparametric tests (Kruskal–Wallis H or one-way ANOVA as appropriate) did not detect statistically significant differences between stages (all $P > 0.05$), likely reflecting limited sample size and high inter-sample variability. (Fig. 1C–E; Supplementary Table 3). To further characterise immune cell interactions during CRC progression, we performed cell–cell communication analysis at each disease stage. From Stage I to Stage II (Fig. 1F and G), T/NK cell signalling activity increased, but subsequently declined during Stages III and IV. Notably, the macrophage migration inhibitory factor (MIF) signalling pathway remained consistently

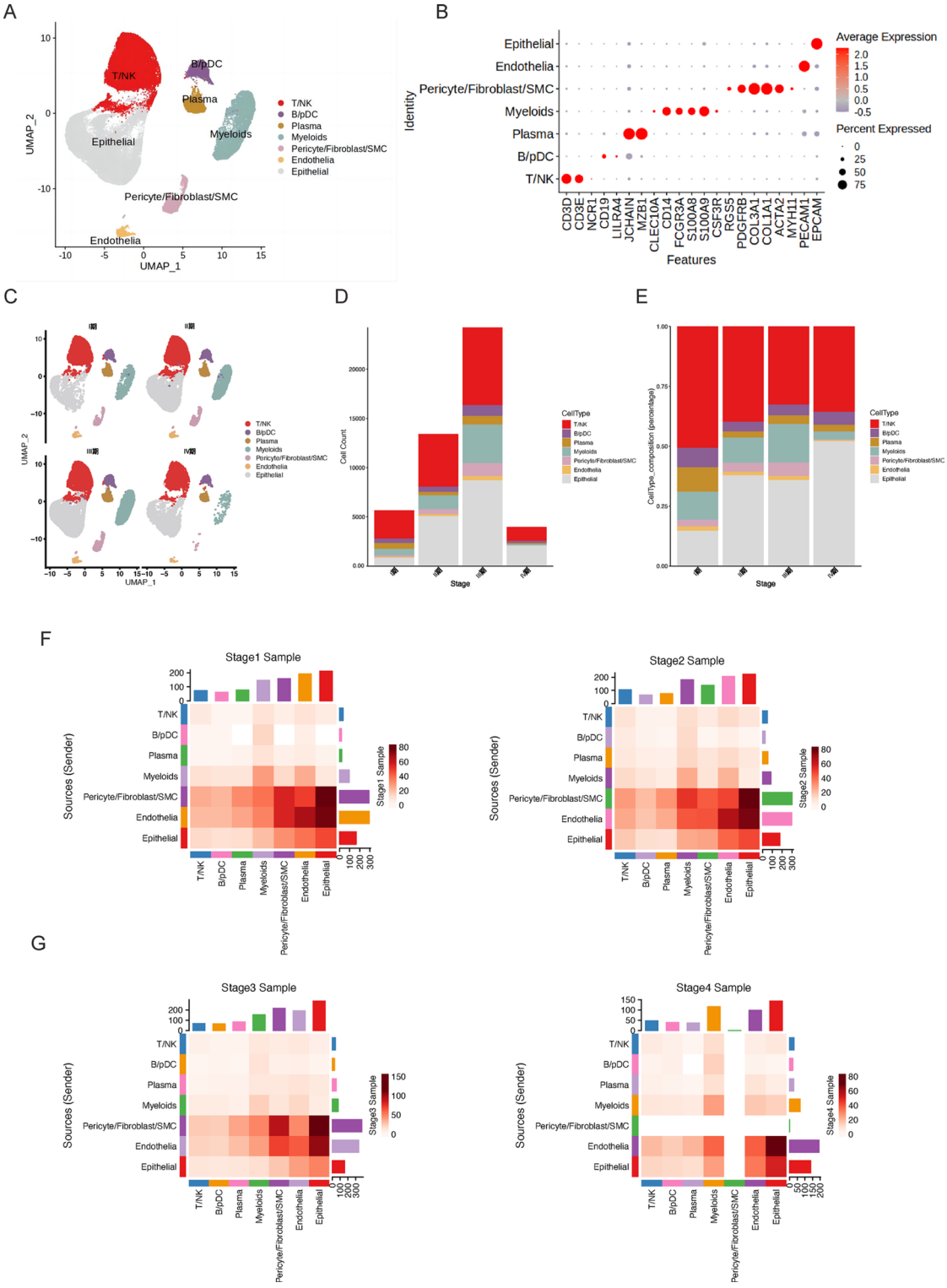


**Fig. 1**. Identification of Seven TME-Associated Cell Subsets in Colorectal Cancer by scRNA-seq. (A) UMAP plot displaying the major cell types identified. (B) Dot plot showing key marker gene expression across cell types; dot size indicates cell proportion, and colour intensity indicates average expression. (C) UMAP plot of immune cell distribution across the TME from Stage I to Stage IV. (D–E) Bar plots illustrating dynamic changes and relative proportions of cell populations and T cell subsets across Stages I to IV. (F) Interaction strength among TME-associated cell subsets in early-stage CRC (Stages I–II). (G) Interaction strength among TME-associated cell subsets in advanced-stage CRC (Stages III–IV).TME, tumour microenvironment; scRNA-seq, single-cell RNA sequencing; UMAP, Uniform Manifold Approximation and Projection; T, T cells; NK, natural killer cells; PD−1, programmed cell death protein 1; Tim−3, T cell immunoglobulin and mucin-domain containing−3; CD39, ectonucleoside triphosphate diphosphohydrolase−1; CD103, integrin alpha E; TIL, tumour-infiltrating lymphocyte; TPM, transcripts per million.

active across all stages (Supplementary Fig. 1 C,1D). These findings suggest that the roles and responsiveness of immune cells within the TME evolve dynamically as CRC progresses.

## Expression of PD-1, TIM-3, and CD103 in T cell subsets

T and NK cells are widely distributed throughout the CRC TME. To systematically characterise the expression of immune checkpoint molecules (PD-1, Tim-3), functional markers (CD39, CD103), and tissue-residency signatures in these subsets, we performed high-resolution clustering based on lineage-defining marker genes, identifying 13 distinct T/NK cell clusters (Fig. 2A and B; Supplementary Table 3).

Comparative analysis across CRC stages (I–IV) revealed dynamic shifts in T cell subset composition (Fig. 2C and D). Th17 cells accounted for 26.79% (IQR 20.9–32.5%) in Stage IV—slightly higher than in earlier stages—yet nonparametric testing did not reveal statistically significant differences between stages ($P > 0.05$) (Fig. 2E; Supplementary Table 4). We further characterised the expression of PD-1, Tim-3, CD39, and CD103 across these T/NK cell subsets (Fig. 2F).

Given the pivotal role of immune checkpoints in regulating $CD8^+$ T cell responses within the TME—particularly in restoring their cytotoxic potential through checkpoint blockade[32,33]—we focused our analysis on $CD8^+$ T cells. Using pseudotime trajectory analysis, $CD8^+$ T cells were mapped into three nodes and six transitional states, illustrating their differentiation from naïve/central memory ($CD8^+$ T-naive/cm) cells into effector ($CD8^+$ Teff) and ultimately exhausted ($CD8^+$ Tex) phenotypes upon tumour antigen exposure (Fig. 2G and H). We then profiled the expression dynamics of key immune regulators (PDCD1, HAVCR2, ENTPD1, and ITGAE) along the $CD8^+$ T cell differentiation trajectory. Three major findings emerged: First, HAVCR2 expression was more strongly enriched than PDCD1 in terminally exhausted $CD8^+$ T cells (Supplementary Fig. 2 A,2B). Second, ENTPD1 peaked during intermediate pseudotime stages and showed partial co-expression with PDCD1, HAVCR2, and ITGAE, suggesting a key role in immunosuppressive transition states (Supplementary Fig. 2 C). Third, ITGAE was predominantly expressed in effector and proliferating $CD8^+$ T cells—consistent with enhanced anti-tumour activity—but also showed secondary enrichment in exhausted subsets (Supplementary Fig. 2D), potentially reflecting tissue residency during chronic antigen stimulation.

Collectively, our findings provide a comprehensive characterisation of the dynamic states of CD8 + T cells in the CRC TME, offering mechanistic insights into T cell exhaustion and potential targets to enhance anti-tumour immunity.

## Expression levels of PD-1, TIM-3, and CD103 are closely related to CRC prognosis

To systematically characterise the spatial distribution and expression profiles of immune checkpoint molecules (PD-1, Tim-3, CD39, and CD103) within the colorectal tumour immune microenvironment, we performed a comprehensive single-cell transcriptomic analysis comprising 371,223 cells retrieved from a publicly available single-cell database. This high-resolution profiling revealed distinct cell-type-specific localisation patterns: PDCD1 was predominantly expressed in T cell subsets and myeloid populations; HAVCR2 was selectively enriched in T lymphocytes; ENTPD1 expression was largely confined to non-epithelial compartments; and ITGAE displayed broad expression across immune lineages, with particularly high levels in T and B cell populations (Fig. 3A). Correlation analysis demonstrated a strong positive association between PDCD1 and HAVCR2 expression in colorectal cancer (partial.rho = 0.598, $P = 1.03 \times 10^{-40}$; partial.rho = 0.569, $P = 2.56 \times 10^{-13}$) (Supplementary Fig. 3 A)[34].

To further explore the immune landscape, we examined the expression and co-expression patterns of PDCD1, HAVCR2, ENTPD1, and ITGAE across defined T and NK cell subsets. Notably, $PLZF^+$ T cells exhibited prominent co-expression of HAVCR2, ENTPD1, and ITGAE. In contrast, PDCD1 showed distinct enrichment in $CD4^+$ T follicular helper (TFH) cells, while the other checkpoint molecules were expressed at relatively low levels in this subset. Moreover, co-expression of all four checkpoint molecules was observed in $CD8^+CXCL13^+HSP^+$ and $CD8^+CXCL13^+$proliferative subsets, both marked by elevated CXCL13 expression (Fig. 3B).

Mismatch repair (MMR) status is a pivotal molecular determinant in colorectal cancer (CRC), distinguishing deficient MMR (dMMR/MSI-H) from proficient MMR (pMMR/MSS) tumours, which are characterised by distinct immune microenvironments and treatment responses. We therefore compared the expression of PDCD1, HAVCR2, ENTPD1, and ITGAE between dMMR and pMMR tumours. All four molecules were more highly expressed in the dMMR group (Fig. 3C). Specifically, PDCD1 expression was significantly elevated in dMMR tumours compared to pMMR tumours (dMMR: 0.80, 95% CI: 0.68–0.91; pMMR: 0.65, 95% CI: 0.53–0.77; $P < 0.05$). Although HAVCR2 and ENTPD1 expression levels were also higher in dMMR tumours, the differences did not reach statistical significance ($P > 0.05$). In contrast, ITGAE expression was significantly increased in dMMR tumours (dMMR: 1.18, 95% CI: 1.10–1.27; pMMR: 0.99, 95% CI: 0.97–1.06; $P < 0.001$) (Fig. 3D).Patients were subsequently stratified based on *MLH1* methylation status into MLH1-methylated (MLH1Meth) and MLH1-unmethylated (MLH1NoMeth) groups. An additional three-group classification was applied: MSS, MSI_MLH1Meth, and MSI_MLH1NoMeth. Expression levels of PDCD1, HAVCR2, ENTPD1, and ITGAE significantly differed between the MSS and MSI_MLH1NoMeth groups. Notably, ITGAE expression was significantly higher in the MLH1Meth group compared to the MLH1NoMeth group (MLH1Meth: 1.20, 95% CI: 1.09–1.31; MLH1NoMeth: 1.00, 95% CI: 0.91–1.09; $P < 0.05$), indicating a statistically significant difference (Supplementary Fig. 3B, 3 C).

Using the UALCAN database[35,36](https://ualcan.path.uab.edu/), we further validated that PDCD1, HAVCR2, ENTPD1and ITGAE were significantly overexpressed in CRC, particularly in mucinous adenocarcinoma. ENTPD1 expression was significantly elevated in mucinous adenocarcinoma compared to non-mucinous adenocarcinoma ($P < 0.05$); HAVCR2 expression was markedly higher in mucinous adenocarcinoma relative to other groups ($P < 0.05$); ITGAE expression differed significantly between normal and tumour tissues ($P < 0.05$), but no significant difference was observed between mucinous and non-mucinous adenocarcinoma subtypes.

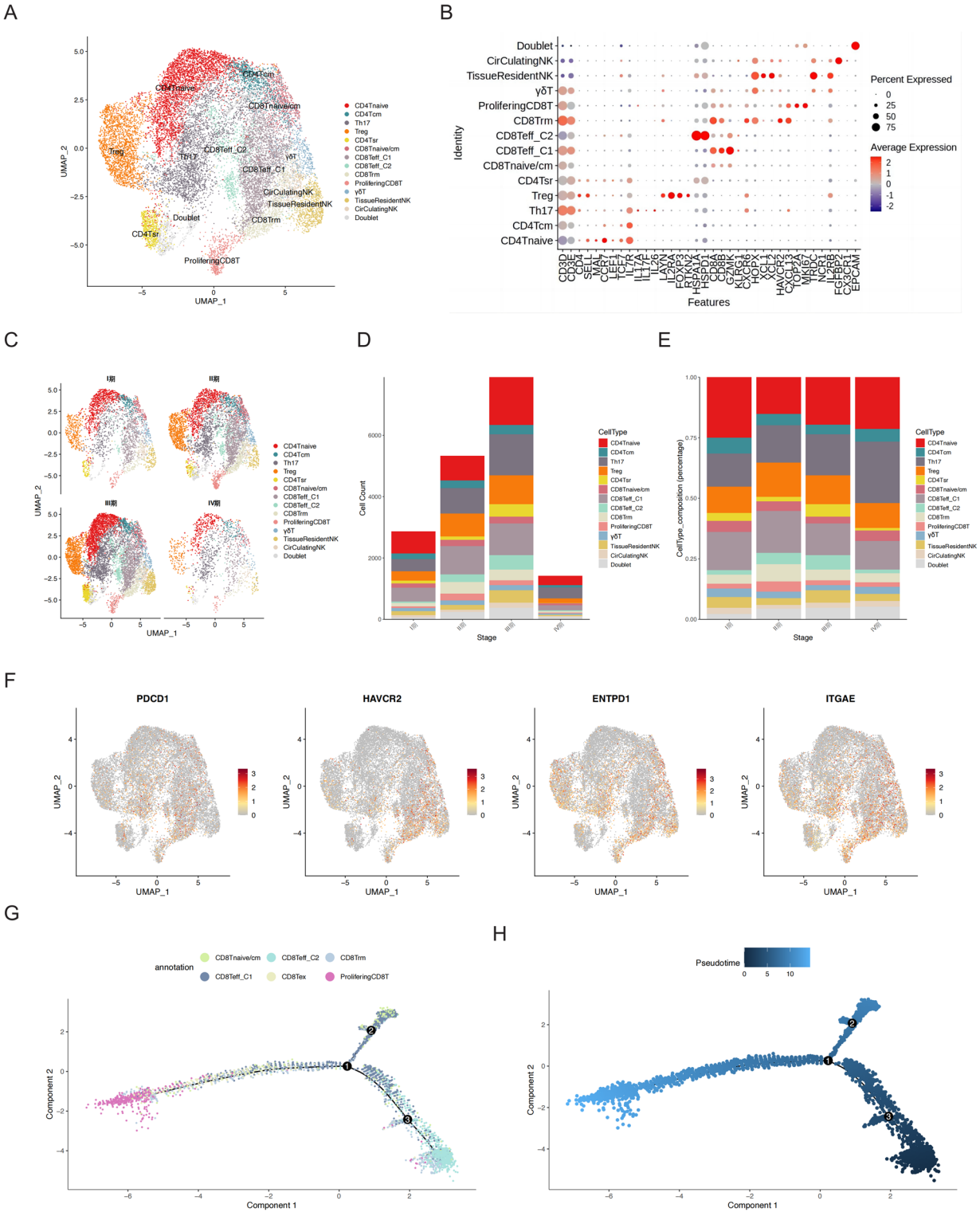


**Fig. 2**. Characterisation of PD−1, Tim−3, CD39 and CD103 Expression in T/NK Cell Subsets (A) UMAP visualisation of T/NK cell subsets.(B) Dot plot displaying expression levels and frequencies of key genes across T/NK cell subtypes. (C) UMAP plots showing T/NK cell distribution and transcriptomic profiles across Stages I–IV. (D–E) Bar plots illustrating dynamic changes and relative proportions of T cell subsets across Stages I to IV.(F) UMAP plots showing expression patterns of PDCD1, HAVCR2, ENTPD1, and ITGAE. (G–H) Differentiation trajectory of $CD8^+$ T cells visualised by cluster identity (G) and pseudotime (H).UMAP, Uniform Manifold Approximation and Projection; T, T cells; NK, natural killer cells; PDCD1, programmed cell death protein 1; HAVCR2, hepatitis A virus cellular receptor 2; ENTPD1, ectonucleoside triphosphate diphosphohydrolase 1; ITGAE, integrin alpha E.

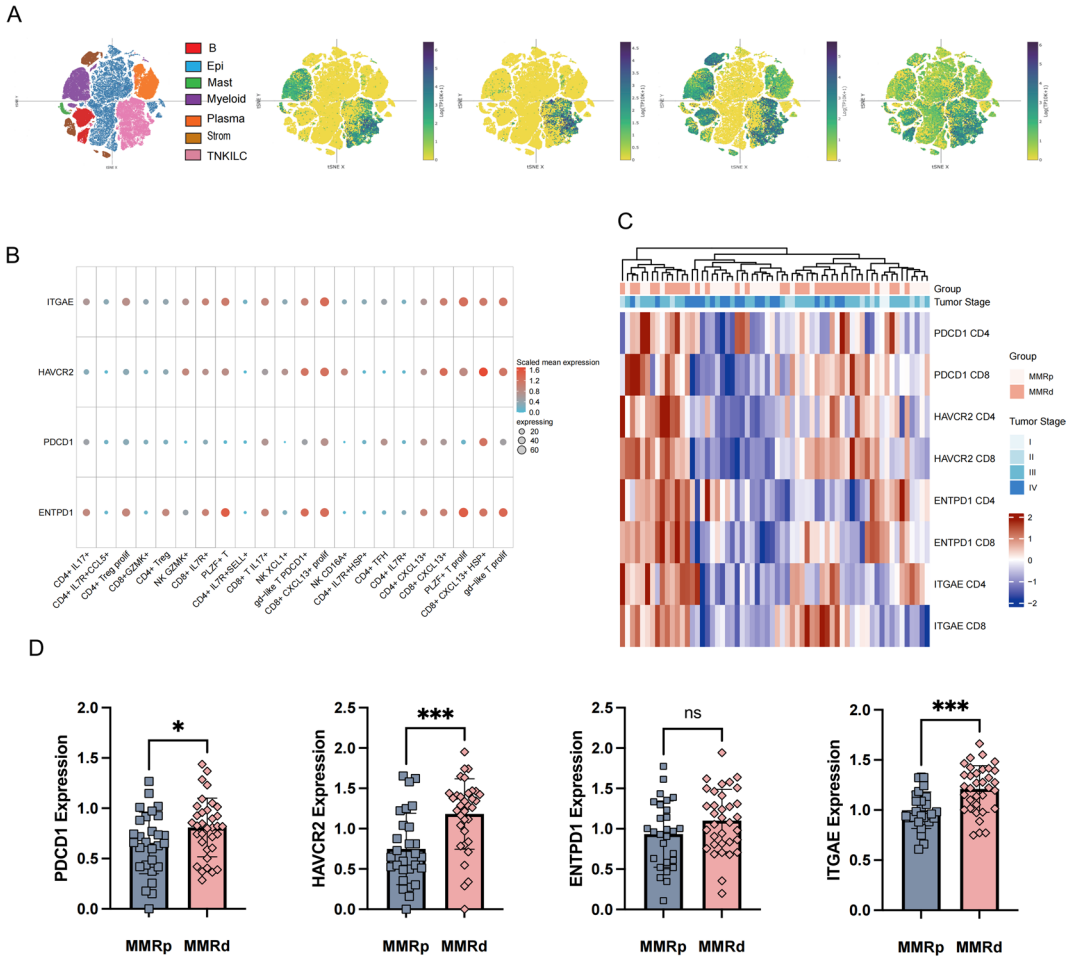


**Fig. 3**. PDCD1, HAVCR2, ENTPD1, and ITGAE Expression in MSS and MSI Colorectal Cancer: Clinical and Prognostic Insights. (A) UMAP visualisation of PDCD1, HAVCR2, ENTPD1, and ITGAE expression in CRC patients. (B) Expression levels of PDCD1, HAVCR2, ENTPD1, and ITGAE across CD4⁺ T cells, CD8⁺ T cells, and NK cell subsets. (C) Hierarchical clustering heatmap showing the expression profiles of PDCD1, HAVCR2, ENTPD1, and ITGAE, with row-wise Z-score normalisation. (D) Comparative expression of PDCD1, HAVCR2, ENTPD1, and ITGAE between MMRp and MMRd CRC patients.two-tailed unpaired Student's t-testswas used in D, $*p<0.05$, $**p<0.01$, $***p<0.001$.CRC, colorectal cancer; PDCD1, programmed cell death protein 1; HAVCR2, hepatitis A virus cellular receptor 2; ENTPD1, ectonucleoside triphosphate diphosphohydrolase 1; ITGAE, integrin alpha E; MSS, microsatellite stable; MSI, microsatellite instability; MMRp, mismatch repair proficient; MMRd, mismatch repair deficient; UMAP, Uniform Manifold Approximation and Projection; NK, natural killer; Z-score, standard score.

(Supplementary Fig. 3D-G). Finally, survival analysis using the Kaplan–Meier Plotter database revealed that higher expression of PDCD1, HAVCR2, and ENTPD1 was associated with shorter overall survival (OS) and relapse-free survival (RFS), whereas elevated ITGAE expression was linked to improved prognosis[37] (Supplementary Fig. 3D-G). Collectively, these findings suggest that while individual immune checkpoint molecules may offer prognostic value, reliance on a single biomarker may be insufficient for accurate prediction of clinical outcomes.

## Exhausted and tissue-resident phenotypes in tumour tissues

To investigate differences in the CD4⁺ and CD8⁺ T cell compartments, we employed flow cytometry to analyse T cells from our clinical cohort. t-SNE was used to visualise the distribution of PD-1, Tim-3, CD39, and CD103 expression across peripheral blood mononuclear cells (PBMCs), adjacent normal tissue (P), and tumour tissue (T) (Fig. 4A–C). Expression of all four immune checkpoint molecules was markedly higher in both P and T tissues compared to PBMCs, suggesting enhanced immune checkpoint activity within the TME. Notably, PD-1, Tim-3, CD39, and CD103 expression was barely detectable on CD8⁺ T cells derived from peripheral blood, but significantly upregulated in both the peritumoural and tumour-infiltrating CD8⁺ T cell populations (Fig. 4D, E).

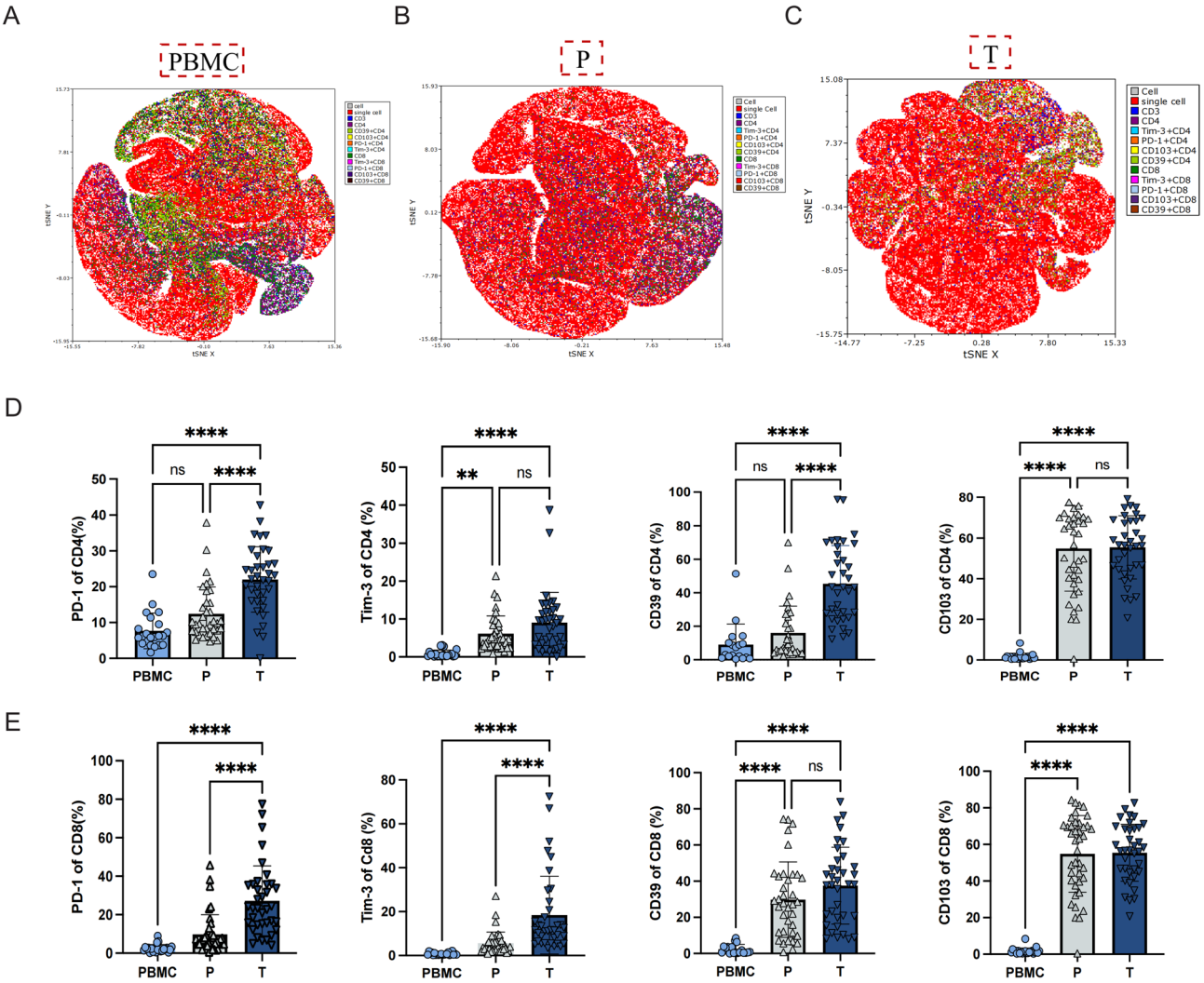


**Fig. 4**. Flow Cytometry Analysis of Different T Cell Phenotypes. (A-C) t-SNE visualization of CD4 + T and CD8 + T cells in immune compartments, categorized by source. (D) Frequencies of PD-1, Tim-3, CD39 and CD103 on CD4 + T cells from PBMC, P, and T samples. (E) Frequencies of PD-1, Tim-3, CD39 and CD103 on CD8 + T cells from PBMC, P, and T samples. (Data are presented as mean ± SD). t-SNE: t-distributed Stochastic Neighbor Embedding.Depending on data normality and variance homogeneity, ANOVA, Welch's ANOVA, or Kruskal–Wallis test with appropriate post hoc comparisons was used in D and E. $^{*}p < 0.05$, $^{**}p < 0.01$, $^{***}p < 0.001$.t-SNE, t-distributed stochastic neighbour embedding; PBMC, peripheral blood mononuclear cells; P, peritumoural tissue; T, tumour tissue; CD4, cluster of differentiation 4; CD8, cluster of differentiation 8; PD-1, programmed cell death protein 1; Tim-3, T cell immunoglobulin and mucin-domain containing-3; CD39, ectonucleoside triphosphate diphosphohydrolase-1; CD103, integrin αE.

## Advanced CRC patients exhibit a more immunosuppressive microenvironment

Given the substantial heterogeneity in PD-1, Tim-3, CD39, and CD103 expression across tissue compartments, we next sought to assess the expression dynamics of these immune checkpoints across different clinical stages. Patients were stratified according to TNM stage, and a progressive decline in T cell abundance was observed with advanced-stage CRC. Notably, Stage I colorectal cancer (CRC) patients exhibited a significantly higher frequency of $CD103^{+}CD8^{+}$ T cells compared to those with more advanced-stage CRC (Fig. 5A).

Further analysis revealed that, relative to PBMCs and P, both $CD8^{+}$ and $CD4^{+}$ Trm cells were more likely to express PD-1 within tumour tissues (T). The $CD39^{+}CD103^{+}$ dual-positive phenotype was preferentially enriched in $CD8^{+}$ T cell subsets compared to $CD4^{+}$ counterparts, suggesting subset-specific roles in the TME (Fig. 5B and C). Flow cytometric profiling of $CD8^{+}$ T cells further demonstrated a marked reduction in their abundance in advanced-stage CRC, accompanied by decreased expression of immune checkpoints including PD-1, Tim-3, CD39, and CD103. Among these, the downregulation of CD103 was particularly pronounced (Stage III–IV: 95% CI: 49.83 [42.30–57.37] vs. Stage I–II: 95% CI: 60.37 [53.10–67.65]; $P < 0.05$) (Fig. 5D).

Based on the combinatorial expression of PD-1, Tim-3, CD39, and CD103, we defined four distinct $CD8^{+}$ T cell subsets: (i) Tex cells ($PD\text{-}1^{+}Tim\text{-}3^{+}CD103^{+}CD8^{+}$), (ii) pf-Trm cells ($PD\text{-}1^{+}Tim\text{-}3^{-}CD103^{+}CD8^{+}$), (iii) tumour-reactive $CD8^{+}$ T cells (including $CD39^{+}CD103^{+}$ and $CD39^{+}CD103^{-}$), and (iv) bystander $CD8^{+}$T cells

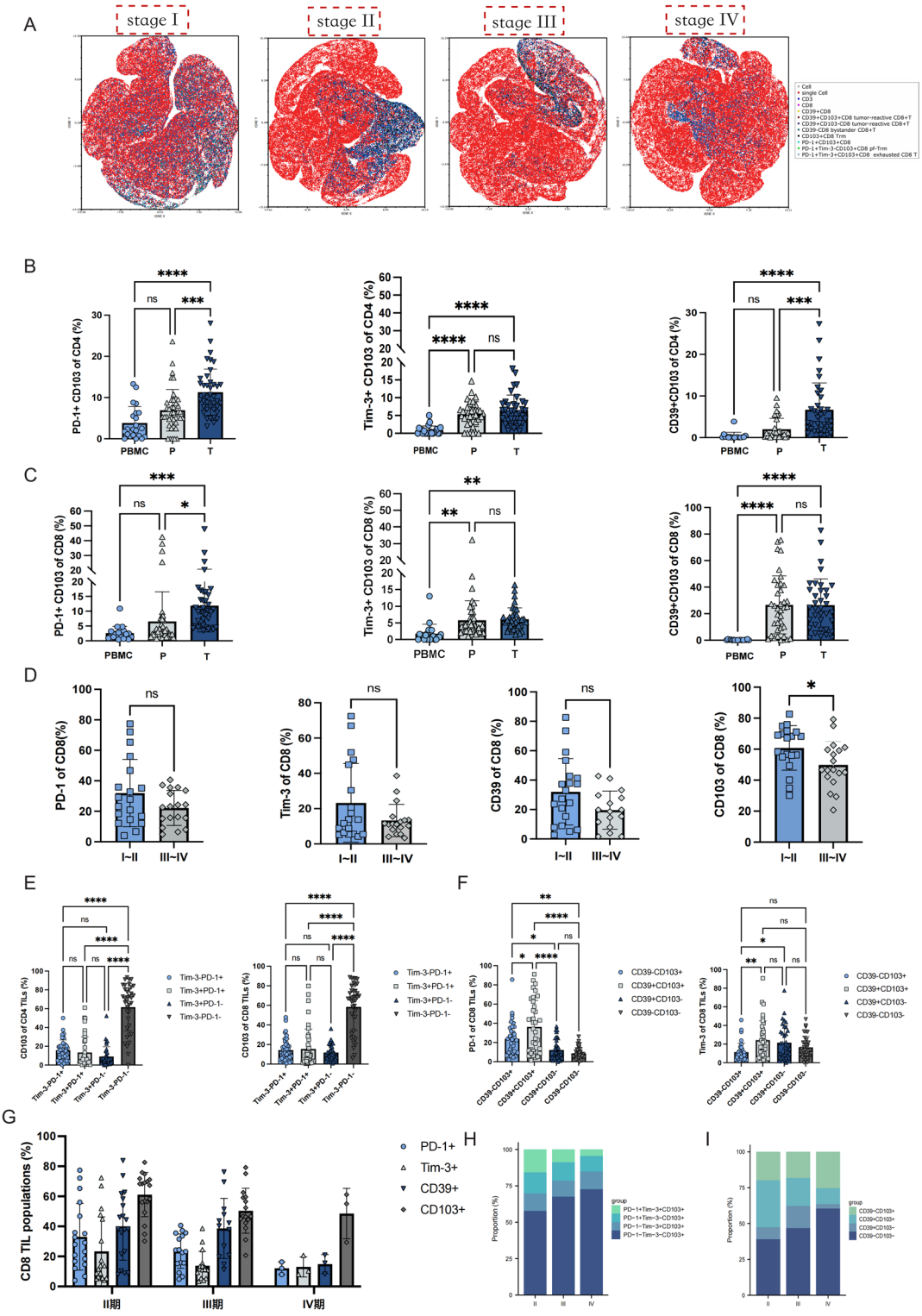


(CD39$^-$CD103$^+$ and CD39$^-$CD103$^-$). We then assessed the distribution of these subsets across clinical stages. Interestingly, most CD103$^+$CD8$^+$ and CD103$^+$CD4$^+$ tumour-infiltrating lymphocytes (TILs) lacked detectable expression of PD-1 and Tim-3 (Fig. 5E). In contrast, CD39$^+$CD103$^+$CD8$^+$ TILs exhibited markedly higher expression of both PD-1 and Tim-3—features commonly associated with tumour-reactive CD8$^+$ T cells (Fig. 5F).

To further visualise checkpoint dynamics during CRC progression, we generated a composite expression plot (Fig. 5G).This analysis revealed a stage-dependent decline in the proportions of Tex cells, pf-Trm cells, tumour-reactive CD8$^+$ T cells, and bystander CD8$^+$ T cells, accompanied by a reciprocal increase in CD8$^+$ T cells lacking all four markers (PD-1, Tim-3, CD39, CD103). Notably, CD39$^+$CD103$^+$ CD8$^+$ T cells were significantly more abundant in Stages I–II (32.8 ± 22.8%) than in Stages III–IV (18.2 ± 12.6%; $P < 0.05$)(Supplementary Fig. 4A-B). No other inter-stage comparisons reached statistical significance (all $P > 0.05$) (Fig. 5H and I; Supplementary Table 4).

◀**Fig. 5**. Cell Dynamics of tex, pf-Trm, tumour-reactive CD8⁺ T cells and bystander CD8⁺ T cells in Tumour Tissues During CRC Progression. (A) t-SNE plots illustrating the distribution of CD8⁺ T cells across Stage I to IV CRC, stratified by TIL enrichment based on PD-1, Tim-3, CD39, and CD103 expression. Tex, pf-Trm, Tumour-reactive CD8⁺ T cells and bystander CD8⁺ T cells populations are highlighted. (B) Frequency of PD-1, Tim-3, and CD39 within CD103⁺CD4⁺ subsets. (C) Frequency of PD-1, Tim-3, and CD39 within CD103⁺CD8⁺ subsets. (D) PD-1, Tim-3, and CD103 expression in CD8⁺ T cells in early (Stages I–II) vs. advanced (Stages III–IV) CRC.(E) Expression levels of Tim-3⁻PD-1⁺, Tim-3⁺PD-1⁺, Tim-3⁺PD-1⁻, and Tim-3⁻PD-1⁻ subsets within CD103⁺CD4⁺ T cells, and pf-Trm (Tim-3⁻PD-1⁺), Tex (Tim-3⁺PD-1⁺), Tim-3⁺PD-1⁻ within CD103⁺CD8⁺ T cells in CRC patients. (F) Expression levels of PD-1 and Tim-3 in tumour-reactive CD8⁺ T cells and bystander CD8⁺ T cells in CRC patients.(G) Expression levels of PD-1, Tim-3, CD39, and CD103 across CRC Stages II, III, and IV. (H) Proportions of Tex (PD-1⁺Tim-3⁺CD103⁺) and pf-Trm (PD-1⁺Tim-3⁺CD103⁻) among CD8⁺ T cells.(I) Proportions of tumour-reactive CD8⁺ T cells (CD39⁺CD103⁺ and CD39⁺CD103⁻) and bystander CD8⁺ T cells (CD39⁻CD103⁺ and CD39⁻CD103⁻).CRC, colorectal cancer; Tex, terminally exhausted T cells; pf-Trm, precursor exhausted tissue-resident memory T cells; Trm, tissue-resident memory T cells; TIL, tumour-infiltrating lymphocyte; PD-1, programmed cell death protein 1; Tim-3, T cell immunoglobulin and mucin-domain containing-3; CD39, ectonucleoside triphosphate diphosphohydrolase-1; t-SNE, t-distributed stochastic neighbor embedding. Data shown as mean ± SD. Depending on data normality and variance homogeneity, ANOVA, Welch's ANOVA, or Kruskal–Wallis test with appropriate post hoc comparisons was used in B, C and E. Two-tailed unpaired Student's t-tests was used in D, $^{*}P < 0.05$, $^{**}P < 0.01$, $^{***}P < 0.001$.

## pf-Trm is associated with poor clinical prognosis in advanced CRC

T cell exhaustion represents a distinct differentiation state driven by chronic antigen stimulation and is characterised by dynamic transitions across multiple cellular states. The relationships and degrees of overlap among these states remain an area of intense investigation. To explore the biological roles and associated signalling pathways of Tex and pf-Trm cells during CRC progression, we stratified cells based on the expression of PD-1, Tim-3, and CD103 into three subsets: CD8⁺ Tex cells, CD8⁺ pf-Trm cells, and proliferating CD8⁺ T cells (Fig. 6A). However, no significant differences in subset proportions were observed across clinical stages, which may be attributed to the limited cell numbers analysed (Fig. 6B).

We next examined the transcriptional profiles of these subsets by identifying differentially expressed genes (DEGs), followed by functional enrichment analysis of upregulated genes. GO analysis revealed that Tex cells were significantly enriched in processes including "viral process," "response to endoplasmic reticulum stress," and "regulation of T cell activation." In contrast, CD8⁺ pf-Trm cells showed enrichment in pathways such as "integrin-mediated cell–cell adhesion," "B cell activation," and the "humoral immune response" (Fig. 6C). KEGG pathway analysis further indicated that Tex cells were enriched in the "T cell receptor signalling pathway," "Th1/Th2 cell differentiation," and the "PD-1 checkpoint pathway," consistent with their exhausted phenotype under chronic antigen exposure (Fig. 6D). Meanwhile, advanced-stage Tex cells showed increased activity in apoptosis-associated pathways such as "regulation of apoptotic signalling" and "endoplasmic reticulum stress response," alongside downregulation of "T cell activation" and "migration" pathways—indicating a marked decline in functional T cell competence (Supplementary Fig. 5A). Similarly, pf-Trm cells were enriched in "antigen processing and presentation," "apoptosis," and "chemokine signalling pathways," underscoring their potential roles in immune surveillance, tissue retention, and cell survival.Further stratification by CRC stage revealed that advanced-stage pf-Trm cells were upregulated in pathways related to "hormone response" and "apoptotic signalling," but exhibited reduced enrichment in pathways governing "antigen presentation" and "immune activation," suggesting impaired immune function and diminished tumour interaction capacity (Supplementary Fig. 5B).

To evaluate the prognostic significance of these subsets, we leveraged transcriptomic data from The Cancer Genome Atlas (TCGA). high Tex frequencies predicted poorer prognosis across all clinical stages (Fig. 6E and F). whereasElevated pf-Trm abundance was associated with significantly improved overall survival (OS) in early-stage patients (Fig. 6G and H), Taken together, these findings highlight stage-specific prognostic associations for distinct CD8⁺ T cell subsets in CRC. While pf-Trm cells confer early protective effects that diminish with tumour progression, accumulation of Tex cells consistently reflects a detrimental immune landscape.

In summary, distinct functional states of CD8⁺ T cells exhibit divergent prognostic implications in CRC, underscoring the importance of subset-specific immune profiling in informing CRC outcomes and therapeutic strategies.

## Discussion

The escalating global burden of colorectal cancer (CRC) underscores the urgent need to characterise the dynamic features of T cells within the TME. Chronic antigen stimulation drives CD8⁺ tumour-infiltrating lymphocytes (TILs) into a state of exhaustion, characterised by diminished effector function, upregulation of co-inhibitory receptors (PD-1, CTLA-4, Tim-3), and reduced cytokine secretion capacity[38]. Notably, the molecular signatures of exhausted T cells carry dual clinical relevance: they not only serve as predictive biomarkers for the efficacy of immune checkpoint inhibitors (ICIs) but also represent actionable therapeutic targets. ICIs reinvigorate antitumour responses by blocking inhibitory signals, thereby preferentially rescuing precursor exhausted CD8⁺ T cells, enhancing their peripheral expansion and tumour infiltration[38]. Consequently, accurate mapping of exhaustion trajectories—particularly the identification of rejuvenatable precursor subsets—will be critical for refining immunotherapeutic strategies in CRC.

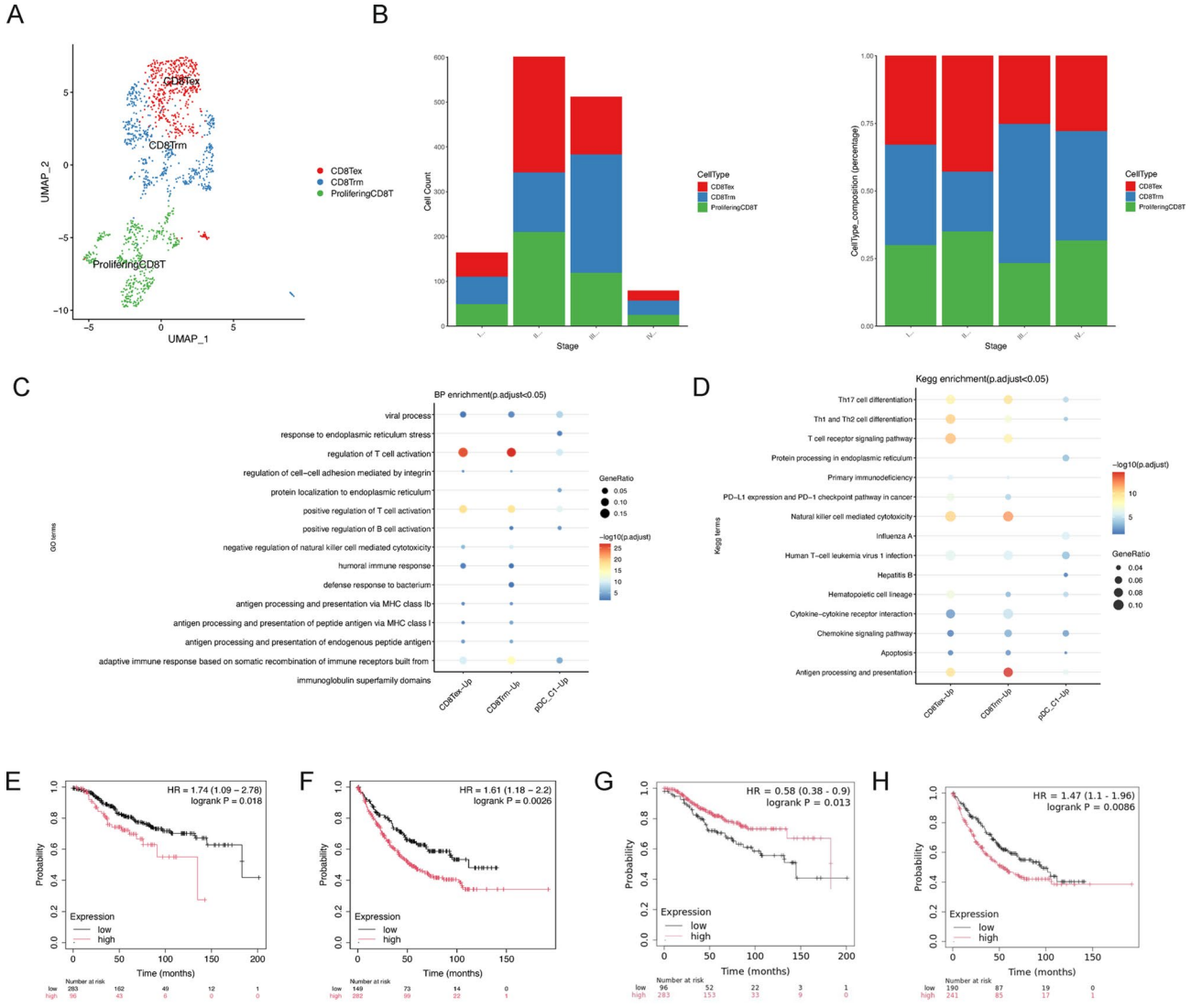


**Fig. 6**. Functional Changes in Tex and pf-Trm in Early and Advanced Stages. (A)UMAP visualization and transcriptomes of CD8 Tex, CD8 pf-Trm, and proliferating CD8 T cells. (B) Dynamic changes in CD8 Tex, CD8 pf-Trm, and proliferating CD8 T cells from Stage I to IV. (C) BP enriched by upregulated genes in Tex and pf-Trm cells. (D) KEGG pathways enriched by upregulated genes in Tex and pf-Trm cells. (E-F) Survival curves for Tex in early (E) and advanced (F) CRC stages. (G-H) Survival curves for pf-Trm in early (G) and advanced (H) CRC stages.Tex, terminally exhausted T cells; pf-Trm, precursor exhausted tissue-resident memory T cells; t-SNE, t-distributed stochastic neighbor embedding; TIL, tumour-infiltrating lymphocyte; PD-1, programmed cell death protein 1; KEGG, Kyoto Encyclopedia of Genes and Genomes; BP, biological process; CRC, colorectal cancer.

Single-cell transcriptomic analysis revealed a progressive decline in the relative abundance of T and NK cells within the TME as CRC advances from stage I to stage IV. Strikingly, myeloid cells and pericyte/fibroblast/smooth muscle cell (SMC) populations also exhibited a marked reduction in stage IV CRC, whereas epithelial cells underwent significant expansion. As previously reported, both tumour cells and the TME are dynamic entities. With tumour progression, interactions between malignant and non-malignant components—including immune and stromal cells—continually evolve, modulating both intrinsic and extrinsic tumour processes[5,39]. To better understand the dynamic remodelling of the CRC immune landscape, we conducted a cell–cell interaction analysis, which revealed fluctuating interaction intensities between T/NK cells and other cellular compartments throughout disease progression. We propose that stage-specific TMEs give rise to distinct infiltration patterns and functional states of tumour-infiltrating T cells. In line with previous studies, stromal and epithelial compartments exhibited consistently strong interaction intensities throughout disease progression. This persistent stromal–epithelial crosstalk, driven by extracellular matrix (ECM) remodelling and associated signalling cascades, likely cooperates to promote tumour malignancy during colorectal cancer progression[40]. Notably, our data reveal sustained activation of the MIF signalling pathway throughout colorectal cancer progression. Consistent with this, previous studies have shown that MIF promotes metabolic reprogramming

and contributes to chemoresistance in colorectal cancer via upregulation of CXCR7, a mechanism linked to poor clinical outcomes[41].

In this study, we identified a CD8⁺ Teff_C1 subset within the TME characterised by high expression of GZMK, alongside concurrent enrichment of Th17 cells. This coordinated presence suggests a transition of the advanced-stage TME towards a state of chronic inflammation and immune tolerance, potentially reflecting a state of partial T cell dysfunction or "pre-exhaustion"[42–45]. Pseudotime trajectory analysis further revealed that CD8⁺ Teff_C2 cells upregulated exhaustion-related markers at terminal stages. Although PD-1, Tim-3, CD39, and CD103 were expressed at various phases of the exhaustion continuum, their levels varied across the trajectory, consistent with previous reports indicating that chronic tumour antigen exposure drives effector T cell exhaustion and impairs antitumour immunity[46,47].

Using single-cell RNA sequencing data, we systematically evaluated the differential expression patterns of PD-1, Tim-3, CD39, and CD103 in microsatellite stable (MMRp) versus microsatellite instability-high (MMRd) colorectal cancer patients.Notably, a single-cell RNA-sequencing study in human melanoma demonstrated that more than one-third of CD8⁺ tumour-infiltrating lymphocytes (TILs) exhibited gene signatures associated with T cell dysfunction, including PDCD1, ENTPD1, LAG3, HAVCR2, ITGAE, CXCL13, TNFRSF9, and proliferation-related genes—yet paradoxically maintained enhanced proliferative potential[48].

In our dataset, PDCD1, HAVCR2, ENTPD1, and ITGAE were more highly expressed in MMRd patients, supporting the notion that checkpoint molecules associated with T cell dysfunction are more readily upregulated in the context of MMR deficiency. This likely reflects a heightened and sustained antigen presentation environment in MMRd tumours, leading to T cell overactivation and subsequent immune checkpoint upregulation as an immune escape mechanism[49]. Additionally, we observed that PD-1, Tim-3, CD39, and CD103 were predominantly expressed on CXCL13⁺ CD8⁺ T cells. This pattern may indicate a positive feedback loop driven by multiple sources of CXCL13 within the TME, reinforcing the expression of exhaustion markers on these cells[50]. Previous studies have shown that T follicular helper (TFH) cells persist in chronic LCMV infection models, with intermediate levels of CXCR5 and PD-1 expression relative to non-TFH and effector TFH cells[51]. Similarly, in CRC, we identified a population of PD-1⁺ CD4⁺ TFH-like cells that may contribute to TME remodelling[52].

To validate these findings, we analysed the expression patterns of PD-1, Tim-3, CD39, and CD103 across different tissue origins and clinical stages in CRC patient cohorts. We observed varying degrees of CD8⁺ T cell exhaustion, particularly pronounced in advanced-stage CRC. Chronic tumour antigen exposure has been shown to induce exhaustion, initially marked by elevated expression of PD-1, Tim-3, CD39, and CD103, followed by progressive functional impairment. Our comparison of early-versus advanced-stage pf-Trm and Tex populations supports this: as CRC advances, the proportion of Tex and pf-Trm within the TME diminishes, contributing to a progressively immunosuppressive environment. Concurrently, tumour-reactive CD8⁺ T cells become depleted and are replaced by non-specific bystander CD8⁺ T cells, further impairing immune surveillance. Notably, Tim-3 expression demonstrated less pronounced changes than PD-1. While Tim-3 is also implicated in regulating T cell exhaustion, its regulatory dynamics and induction thresholds may differ across TMEs. This discrepancy may reflect PD-1's broader or earlier role in marking T cell dysfunction[53].

Building on the quantification of Tex and pf-Trm cell populations across different stages of colorectal cancer (CRC), we investigated their respective functional roles within the tumour immune microenvironment. By identifying differentially expressed genes between early and advanced disease stages and performing subsequent GO and KEGG enrichment analyses, we found that CD8⁺ Tex cells were predominantly enriched for pathways associated with chronic antigenic stimulation, T cell receptor (TCR) signalling, and PD-1/PD-L1 checkpoint regulation—hallmark features of T cell exhaustion. In contrast, CD8⁺ pf-Trm cells were primarily involved in sustaining immune surveillance and facilitating immune–tissue interactions[54,55]. Our results indicate that early-stage Tex cells retain partial effector function, while their advanced-stage counterparts exhibit marked functional impairment, increased apoptotic potential, and heightened cellular stress. This transition is characterised by a shift from a relatively quiescent or responsive state to a terminally dysfunctional phenotype, with a significant reduction in immune competence and upregulation of cell death–related processes. Similarly, early pf-Trm cells displayed robust features of immune surveillance, including antigen presentation, cell adhesion, and responsiveness to environmental cues. However, advanced-stage pf-Trm cells showed elevated expression of stress-response genes, increased vulnerability to apoptosis, and diminished immune function. These alterations suggest a progressive deterioration in their ability to maintain effective tissue residency and protective immunity.

Recent advances in single-cell and multi-omics profiling have provided unprecedented insights into the complex cellular architecture of the tumour microenvironment (TME) in colorectal cancer (CRC)[56–60] and other malignancies such as head and neck squamous cell carcinoma (HNSCC)[61], cervical cancer[62], and prostate cancer[63]. These studies consistently highlight the TME as a highly heterogeneous and dynamic ecosystem shaped by tumour–immune–stromal interactions. A common methodological strength across prior work lies in the use of high-resolution single-cell RNA sequencing, often in conjunction with spatial or genomic approaches, to reveal transcriptional programmes and intercellular cross-talk within tumours. Building upon these foundations, our study offers a unique contribution by integrating single-cell transcriptomic analysis with flow cytometric validation in CRC samples across distinct clinical stages. Specifically, we focus on the dynamic roles of CD8⁺ T cell subpopulations—namely, exhausted T cells (Tex) and peripheral tissue–resident memory T cells (pf-Trm)—during disease progression. Notably, we found that pf-Trm cells in early-stage CRC are associated with improved prognosis, whereas in advanced-stage tumours, their phenotypic shift towards immunosuppressive features correlates with poorer clinical outcomes. This observation suggests a context-dependent functional reprogramming of pf-Trm cells shaped by the evolving TME.

However, our study has several limitations. First, the relatively modest sample size and lack of matched normal controls limit the statistical power and generalizability of our conclusions. Second, although we used

univariable survival models to demonstrate associations, the small number of events precluded adjustment for potential confounders such as disease stage, age, and MMR status; future work will expand the cohort, extend follow-up, and perform multivariable regression—including these key covariates—to validate the independence and robustness of our prognostic findings. Third, while we describe distinct transcriptional phenotypes among Tex, pf-Trm, tumor-reactive CD8⁺ T cells, and bystander CD8⁺ T cells, the developmental relationships and plasticity between these subsets remain unresolved. In summary, our work expands the current understanding of intratumoral T cell diversity by highlighting the prognostic relevance and phenotypic evolution of pf-Trm cells in CRC. These findings underscore the need for a stage-specific perspective when evaluating immune cell function within the TME and point towards pf-Trm cells as potential biomarkers or therapeutic targets. Further mechanistic studies are warranted to validate these observations and clarify their implications for immunotherapy in CRC.

## Data availability

The datasets used and/or analysed during the current study available from the corresponding author on reasonable request.

Received: 24 December 2024; Accepted: 30 July 2025
Published online: 05 August 2025

## References

1. Siegel, R. L., Miller, K. D., Wagle, N. S. & Jemal, A. Cancer statistics, 2023. *CA Cancer J. Clin.* **73**, 17–48 (2023).
2. Bray, F. et al. Global cancer statistics 2022: GLOBOCAN estimates of incidence and mortality worldwide for 36 cancers in 185 countries. *CA Cancer J. Clin.* **74**, 229–263 (2024).
3. Sadeghi, M., Dehnavi, S., Sharifat, M., Amiri, A. M. & Khodadadi, A. Innate immune cells: key players of orchestra in modulating tumor microenvironment (TME). *Heliyon* **10**, e27480 (2024).
4. Gajewski, T. F., Schreiber, H. & Fu, Y. X. Innate and adaptive immune cells in the tumor microenvironment. *Nat. Immunol.* **14**, 1014–1022 (2013).
5. Binnewies, M. et al. Understanding the tumor immune microenvironment (TIME) for effective therapy. *Nat. Med.* **24**, 541–550 (2018).
6. St Paul, M. & Ohashi, P. S. The roles of CD8(+) T cell subsets in antitumor immunity. *Trends Cell. Biol.* **30**, 695–704 (2020).
7. Lowery, F. J. et al. Molecular signatures of antitumor neoantigen-reactive T cells from metastatic human cancers. *Science* **375**, 877–884 (2022).
8. Jhunjhunwala, S., Hammer, C. & Delamarre, L. Antigen presentation in cancer: insights into tumour immunogenicity and immune evasion. *Nat. Rev. Cancer.* **21**, 298–312 (2021).
9. Thommen, D. S. & Schumacher, T. N. T cell dysfunction in cancer. *Cancer Cell.* **33**, 547–562 (2018).
10. Barsch, M. et al. T-cell exhaustion and residency dynamics inform clinical outcomes in hepatocellular carcinoma. *J. Hepatol.* **77**, 397–409 (2022).
11. Harris, M. A. et al. Towards targeting the breast cancer immune microenvironment. *Nat. Rev. Cancer*. **24**, 554–577 (2024).
12. Banchereau, R. et al. Intratumoral CD103 + CD8 + T cells predict response to PD-L1 Blockade. *J. Immunother Cancer*. **9**, e002231 (2021).
13. Najjar, Y. G. et al. Neoadjuvant pembrolizumab and High-Dose IFNα-2b in resectable regionally advanced melanoma. *Clin. Cancer Res.* **27**, 4195–4204 (2021).
14. Webb, J. R., Milne, K., Watson, P., Deleeuw, R. J. & Nelson, B. H. Tumor-infiltrating lymphocytes expressing the tissue resident memory marker CD103 are associated with increased survival in high-grade serous ovarian cancer. *Clin. Cancer Res.* **20**, 434–444 (2014).
15. Li, Q. et al. Recurrence and prognosis in intrahepatic cholangiocarcinoma patients with different etiology after radical resection: a multi-institutional study. *BMC Cancer*. **22**, 329 (2022).
16. Ford, K. et al. NOX4 Inhibition potentiates immunotherapy by overcoming Cancer-Associated Fibroblast-Mediated CD8 T-cell exclusion from tumors. *Cancer Res.* **80**, 1846–1860 (2020).
17. van der Leun, A. M., Thommen, D. S. & Schumacher, T. N. CD8(+) T cell States in human cancer: insights from single-cell analysis. *Nat. Rev. Cancer*. **20**, 218–232 (2020).
18. Sauer, N. et al. TIM-3 as a promising target for cancer immunotherapy in a wide range of tumors. *Cancer Immunol. Immunother.* **72**, 3405–3425 (2023).
19. Miller, B. C. et al. Subsets of exhausted CD8(+) T cells differentially mediate tumor control and respond to checkpoint Blockade. *Nat. Immunol.* **20**, 326–336 (2019).
20. Lee, H. O. et al. Lineage-dependent gene expression programs influence the immune landscape of colorectal cancer. *Nat. Genet.* **52**, 594–603 (2020).
21. Duhen, T. et al. Co-expression of CD39 and CD103 identifies tumor-reactive CD8 T cells in human solid tumors. *Nat. Commun.* **9**, 2724 (2018).
22. Chow, A. et al. The ectonucleotidase CD39 identifies tumor-reactive CD8(+) T cells predictive of immune checkpoint Blockade efficacy in human lung cancer. *Immunity* **56**, 93–106e6 (2023).
23. Shen, Y. et al. CD39(hi) identifies an exhausted tumor-reactive CD8(+) T cell population associated with tumor progression in human gastric cancer. *Pharmacol. Res.* **202**, 107122 (2024).
24. Simoni, Y. et al. Bystander CD8(+) T cells are abundant and phenotypically distinct in human tumour infiltrates. *Nature* **557**, 575–579 (2018).
25. van den Bulk, J. et al. CD103 and CD39 coexpression identifies neoantigen-specific cytotoxic T cells in colorectal cancers with low mutation burden. *J. Immunother Cancer*. **11**, e005887 (2023).
26. Pelka, K. et al. Spatially organized multicellular immune hubs in human colorectal cancer. *Cell* **184**, 4734–4752e20 (2021).
27. Kanehisa, M., Furumichi, M., Sato, Y., Matsuura, Y. & Ishiguro-Watanabe, M. KEGG: biological systems database as a model of the real world. *Nucleic Acids Res.* **53**, D672–D677 (2025).
28. Kanehisa, M. Toward Understanding the origin and evolution of cellular organisms. *Protein Sci.* **28**, 1947–1951 (2019).
29. Kanehisa, M. & Goto, S. KEGG: Kyoto encyclopedia of genes and genomes. *Nucleic Acids Res.* **28**, 27–30 (2000).
30. Chen, Y. et al. Epithelial cells activate fibroblasts to promote esophageal cancer development. *Cancer Cell.* **41**, 903–918e8 (2023).
31. Lai, H. et al. Single-cell RNA sequencing reveals the epithelial cell heterogeneity and invasive subpopulation in human bladder cancer. *Int. J. Cancer*. **149**, 2099–2115 (2021).
32. Jiang, W. et al. Exhausted CD8 + T cells in the tumor immune microenvironment: new pathways to therapy. *Front. Immunol.* **11**, 622509 (2020).

33. Lu, L. & Deng, L. TIM-3 inhibitors: a promising strategy for tumor immunotherapy. *Trends Mol. Med.* **30**, 202–203 (2024).
34. Li, T. et al. TIMER2.0 for analysis of tumor-infiltrating immune cells. *Nucleic Acids Res.* **48**, W509–W514 (2020).
35. Chandrashekar, D. S. et al. An update to the integrated cancer data analysis platform. *Neoplasia 25*. **UALCAN**, 18–27 (2022).
36. Chandrashekar, D. S. et al. UALCAN: A portal for facilitating tumor subgroup gene expression and survival analyses. *Neoplasia* **19**, 649–658 (2017).
37. Chen, L. et al. Prognostic values of tissue-resident CD8(+)T cells in human hepatocellular carcinoma and intrahepatic cholangiocarcinoma. *World J. Surg. Oncol.* **21**, 124 (2023).
38. Philip, M. & Schietinger, A. CD8(+) T cell differentiation and dysfunction in cancer. *Nat. Rev. Immunol.* **22**, 209–223 (2022).
39. Chow, A., Perica, K., Klebanoff, C. A. & Wolchok, J. D. Clinical implications of T cell exhaustion for cancer immunotherapy. *Nat. Rev. Clin. Oncol.* **19**, 775–790 (2022).
40. Mun, J. Y., Leem, S. H., Lee, J. H. & Kim, H. S. Dual relationship between stromal cells and immune cells in the tumor microenvironment. *Front. Immunol.* **13**, 864739 (2022).
41. Hu, S., Feng, J., Fu, W. & Guo, Y. Macrophage migration inhibitory factor (MIF) upregulates CXCR7 and contributes to chemotherapy resistance in colorectal cancer. *Cell. Biochem. Biophys.* **82**, 3437–3452 (2024).
42. Schmitt, M. & Greten, F. R. The inflammatory pathogenesis of colorectal cancer. *Nat. Rev. Immunol.* **21**, 653–667 (2021).
43. Joeckel, L. T. et al. Mouse granzyme K has pro-inflammatory potential. *Cell. Death Differ.* **18**, 1112–1119 (2011).
44. Li, Z. et al. Exploring GZMK as a prognostic marker and predictor of immunotherapy response in breast cancer: unveiling novel insights into treatment outcomes. *J. Cancer Res. Clin. Oncol.* **150**, 286 (2024).
45. Kimura, A. & Kishimoto, T. Th17 cells in inflammation. *Int. Immunopharmacol.* **11**, 319–322 (2011).
46. Zhang, Z. et al. Cell dysfunction and exhaustion in cancer. *Front. Cell. Dev. Biol.* **8**, 17 (2020).
47. Sekiya, T. & Yoshimura, A. In vitro Th differentiation protocol. *Methods Mol. Biol.* **1344**, 183–191 (2016).
48. Li, H. et al. Dysfunctional CD8 T cells form a proliferative, dynamically regulated compartment within human melanoma. *Cell* **176**, 775–789e18 (2019).
49. Amodio, V. et al. Mechanisms of immune escape and resistance to checkpoint inhibitor therapies in mismatch repair deficient metastatic colorectal cancers. *Cancers (Basel)*. **13**, 2638 (2021).
50. Gao, S. H., Liu, S. Z., Wang, G. Z. & Zhou, G. B. CXCL13 in cancer and other diseases: biological functions, clinical significance, and therapeutic opportunities. *Life (Basel)*. **11**, 1282 (2021).
51. Künzli, M. et al. Long-lived T follicular helper cells retain plasticity and help sustain humoral immunity. *Sci. Immunol.* **5**, eaay5552 (2020). [pii].
52. Künzli, M. & Masopust, D. CD4(+) T cell memory. *Nat. Immunol.* **24**, 903–914 (2023).
53. Fan, L. et al. Targeting pro-inflammatory T cells as a novel therapeutic approach to potentially resolve atherosclerosis in humans. *Cell. Res.* **34**, 407–427 (2024).
54. Losurdo, A. et al. Author correction: Single-cell profiling defines the prognostic benefit of CD39(high) tissue resident memory CD8 + T cells in luminal-like breast cancer. *Commun. Biol.* **4**, 1252 (2021).
55. Cheng, Y. et al. Non-terminally exhausted tumor-resident memory HBV-specific T cell responses correlate with relapse-free survival in hepatocellular carcinoma. *Immunity* **54**, 1825–1840e7 (2021).
56. Khaliq, A. M. et al. Refining colorectal cancer classification and clinical stratification through a single-cell atlas. *Genome Biol.* **23**, 113 (2022).
57. Zhang, Y. et al. Tumor editing suppresses innate and adaptive antitumor immunity and is reversed by inhibiting DNA methylation. *Nat. Immunol.* **25**, 1858–1870 (2024).
58. Zhou, Y. et al. Single-Cell multiomics sequencing reveals prevalent genomic alterations in tumor stromal cells of human colorectal cancer. *Cancer Cell.* **38**, 818–828e5 (2020).
59. Wang, R. et al. Single-cell genomic and transcriptomic landscapes of primary and metastatic colorectal cancer tumors. *Genome Med.* **14**, 93 (2022).
60. Chu, X. et al. Integrative single-cell analysis of human colorectal cancer reveals patient stratification with distinct immune evasion mechanisms. *Nat. Cancer*. **5**, 1409–1426 (2024).
61. Cheng, Y. et al. Single-cell and Spatial RNA sequencing identify divergent microenvironments and progression signatures in early- versus late-onset prostate cancer. *Nat. Aging*. **5**, 909–928 (2025).
62. Jenkins, B. H. et al. Single cell and Spatial analysis of immune-hot and immune-cold tumours identifies fibroblast subtypes associated with distinct immunological niches and positive immunotherapy response. *Mol. Cancer*. **24**, 3 (2025).
63. Bedard, M. C. et al. Single cell transcriptomic analysis of HPV16-infected epithelium identifies a keratinocyte subpopulation implicated in cancer. *Nat. Commun.* **14**, 1975 (2023).


## Author contributions

Author ContributionsHan Wu: Conceptualization，Data curation，Formal analysis，Investigation，Methodology，Validation，Visualization，Writing - original draft；Pei-Wen Fan: Conceptualization，Data curation，Formal analysis，Investigation，Methodology，Validation，Visualization，Writing - review & editing；Ya-Ning Feng: Data curation，Methodology，Validation； Cheng Chang: Formal analysis，Methodology，Validation；Ting Gui: Data curation，Formal analysis；Jia-bei Meng: Data curation，Formal analysis；Ruo-Zheng Wang: Conceptualization，Funding acquisition，Project administration，Resources，Supervision，Writing - review & editing；Han Wu and Pei-Wen Fan made equal contributions to this study.

## Funding

This study was supported by the Shanghai Cooperation Organisation Science and Technology Partnership Programme and International Science and Technology Cooperation Programme (No.2020E01056).

## Declarations

## Competing interests

The authors declare no competing interests.

## Ethical approval

Approval of the research protocol by an Institutional Reviewer Board.

## Informed consent

Informed consents were provided by all the participants.

## Additional information

**Supplementary Information** The online version contains supplementary material available at https://doi.org/10.1038/s41598-025-14409-x.

**Correspondence** and requests for materials should be addressed to R.-Z.W.

**Reprints and permissions information** is available at www.nature.com/reprints.

**Publisher's note** Springer Nature remains neutral with regard to jurisdictional claims in published maps and institutional affiliations.